

TRANSFORMATION RULES ON ENGINEERING STRESS STRAIN CURVES OF S690 FUNNEL-SHAPED COUPONS

H.C. Ho^{1,2*}, K.F. Chung^{1,2} and Y.B. Guo²

¹ Chinese National Engineering Research Centre for Steel Construction (Hong Kong Branch),

The Hong Kong Polytechnic University, Hong Kong SAR

² Department of Civil and Environmental Engineering,

The Hong Kong Polytechnic University, Hong Kong SAR

Emails: hc.ho@polyu.edu.hk, cekchung@polyu.edu.hk, liz.guo@connect.polyu.hk

*Corresponding author

Abstract. *Funnel-shaped coupons are widely adopted for various low cycle high strain cyclic tests to investigate hysteretic behaviour of structural steels in order to avoid plastic axial buckling under cyclic actions. However, a technical problem is induced that the engineering stress strain curves obtained from these funnel-shaped coupons are not comparable to those curves obtained from standard cylindrical coupons. Hence, it is essential to correlate the engineering stress-strain characteristics obtained from monotonic tensile tests using these two types of coupons. This paper presents a theoretical study into such a correlation on the stress strain characteristics between the funnel-shaped coupons and the standard cylindrical coupons. A series of transformation formulae are proposed for various deformation ranges, namely i) Elastic range; ii) Plateau range; iii) Hardening range and iv) Necking range. The proposed transformation formulae have been calibrated with both test and numerical results for the S690 funnel-shaped coupons and the S690 cylindrical coupons. These results provide strong evidence to the effectiveness of the proposed transformation rules for subsequent investigations into hysteretic behaviour of steel materials.*

Keywords: Tensile tests, funnel-shaped coupons, S690 steels, stress-strain characteristics;

1. INTRODUCTION

Hysteretic behaviour of structural members is very important for a seismic resistant structure, which affects heavily its seismic responses under low cycle high strain cyclic actions. It is important to quantify the hysteretic behaviour of both the steel materials and their structural systems against seismic actions. In the past two decades, many researchers (Fournier et al. 2006, Nip et al. 2010) conducted experimental investigations into the hysteretic behaviour of structural steels with different testing methods due to different areas of interest and engineering applications.

In general, funnel-shaped test coupons are commonly adopted for low cycle high strain cyclic tests to BS 3518-3 (1963), GB/T 15248 (1994), and ISO 12106 (2003). However, a technical problem is induced that the engineering stress strain curves obtained from cyclic tests with funnel-shaped coupons are not directly comparable to those curves obtained from these tensile tests with standard cylindrical coupons due to different definitions of gauge lengths and engineering strains. Consequently, it is essential to perform a theoretical analysis to generate

transformation rules for assessment on the stress-strain characteristics of the steel materials tested with funnel-shaped coupons and standard cylindrical coupons.

2. STRESS-STRAIN CHARACTERISTICS OF FUNNEL-SHAPED COUPONS

2.1. Dimensions of cylindrical and funnel-shaped coupons

In general, the cylindrical coupon is considered to be suitable for cyclic tests up to a maximum strain of 2% while the funnel-shaped coupon is considered to be suitable for a strain amplitude between 2% to 15%. A standard cylindrical coupon is of a circular cross-section with tangentially blending fillets between the parallel length and the ends, as shown in Figure 1a. The ends of the coupon should be formed to suit the type of testing machine. The gauge length of a cylindrical coupon is taken as 5 times of the diameter, i.e. $L_o = 5d$.

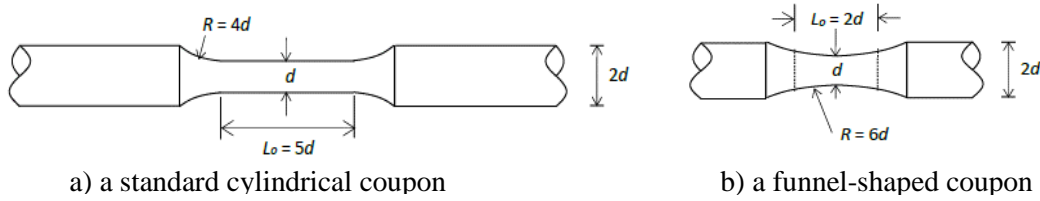


Figure 1. Geometry of coupons

However, a standard funnel-shaped coupon is of a circular cross-section with a continuous varying radius between both ends, as shown in Figure 1b, while the gauge length of the funnel-shaped coupon is taken as twice the diameter, i.e. $L_o = 2d$. In the funnel-shaped region, the radius of curvature is specified as 6 times of the diameter, i.e. $R = 6d$. Hence, the variation in the cross-sectional radius, r , against the longitudinal length, x , can be expressed as the following mathematical formulation:

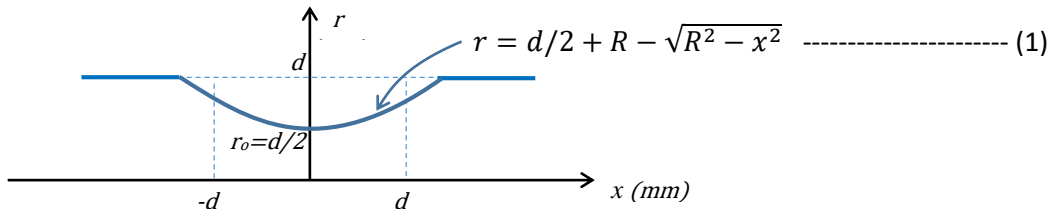


Figure 2. Variation in radius against longitudinal length of a funnel-shaped coupon

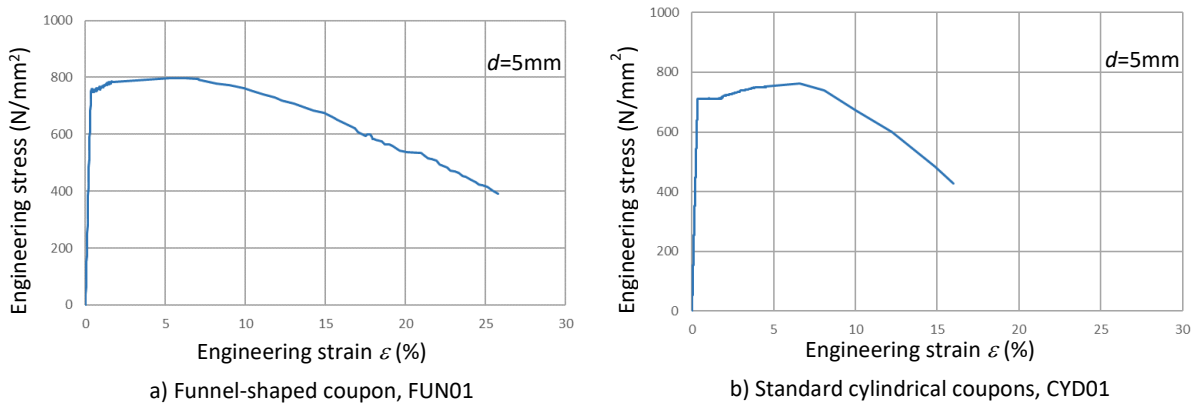


Figure 3. Engineering stress-strain curves of S690 funnel-shaped and cylindrical coupons

2.2 Tensile tests of funnel-shaped and cylindrical coupons

Tensile tests of both funnel shaped and cylindrical coupons of S690 steels were carried out. All coupons are of 5 mm diameter. The measured engineering stress-strain curves are plotted

in Figure 3. Key data and test results are presented in Table 1. The test results will be used for calibration of the proposed analytical method for evaluation of deformations of funnel-shaped coupons under different deformation stages in subsequent sections.

Table 1. Tensile test results of S690 funnel-shaped and cylindrical coupons

Specimen	f_y (N/mm ²)	ε_y (%)	E (kN/mm ²)	f_h (N/mm ²)	ε_h (%)	f_u (N/mm ²)	ε_u (%)	ε_L (%)
FUN01	751	0.36	200	767	0.96	790	5.19	25.78
CYD01	711	0.36	200	716	2.34	753	6.57	16.01

2.3. Deformations of funnel-shaped coupons

The authors (Ho et.al. 2009) carried out a series of research projects to investigate the true stress characteristics of S690 steels using a newly developed Instantaneous Area Method. In general, a typical stress strain curve of high strength S690 steel can be classified into four deformation stages, namely i) Elastic stage; ii) Plateau stage; iii) Hardening stage; and iv) Necking stage, as shown in Figure 4. Typical localized deformations within the gauge length of the funnel-shaped coupon is presented in Figure 5.

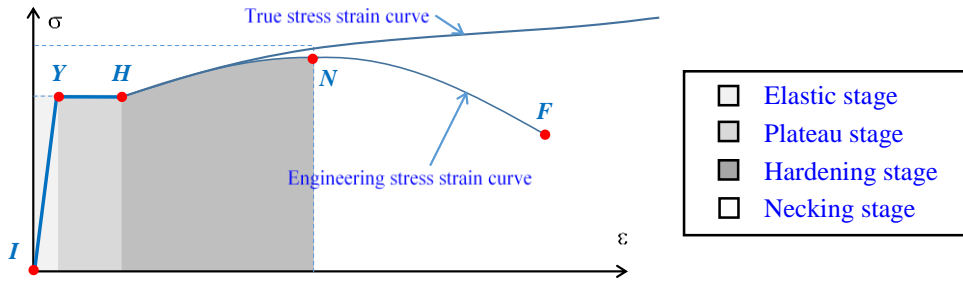


Figure 4. Typical stress strain characteristics of steel materials

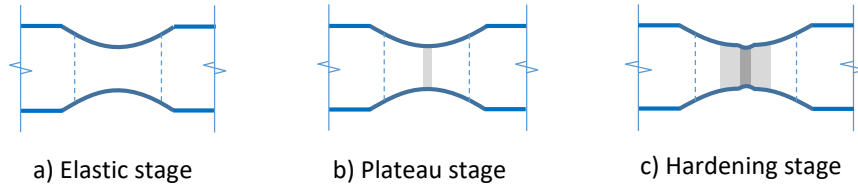


Figure 5. Localized deformations at different deformation ranges

2.3.1 Deformation at the elastic stage

In the elastic stage, all materials of the funnel-shaped coupon are elastic until the stresses within the minimum cross-section reaches the yield strength. Thus, the elongation of the coupon within the gauge length, Δ , is given by

$$\Delta = \sum \frac{\sigma}{E} = 2 \int_0^d \frac{F}{EA} dl = 2 \int_0^d \frac{F}{E\pi r^2} dl = 0.459 \frac{F}{E} \quad (2)$$

For details of the derivation procedures, please refer to Appendix A. Thus, the point of yielding of the coupon is given by:

Stage 1 - Point of yielding, Y:

Stress, $f_y = 751$ N/mm²; Nominal cross-sectional area = 19.63mm²;

$$\Delta = 0.459 \frac{f_y \pi d^2}{E \cdot 4} = 0.459 * \frac{751}{200000} * \frac{25 \pi}{4} = 0.034 \text{ mm}$$

Strain corresponding to Point Y, $\varepsilon_y = 0.034 / 10 \times 100\% = 0.34\%$

2.3.2 Deformation at the plateau stage

After the elastic stage, the deformation enters into the plateau stage, in which limited hardening effect is present locally in the shaded area of the coupon, as shown in Figure 6. At the end of the plateau stage, the stresses within the minimum cross-section reaches f_h , i.e. Point H – Onset of hardening. It is essential to identify the yielding zone of the coupon by direct determination of the critical length, l_c , as illustrated in Figure 6. Based on the stress ratio between f_h and f_y , i.e. f_h/f_y , the critical value of the cross-sectional diameter d_c at which material yielding begins is determined by the principle of force equilibrium.

$$\frac{\pi d_c^2}{4} \cdot f_y = \frac{\pi d^2}{4} \cdot f_h \quad \Rightarrow \quad \therefore \text{critical diameter } d_c = d \sqrt{f_h/f_y}$$

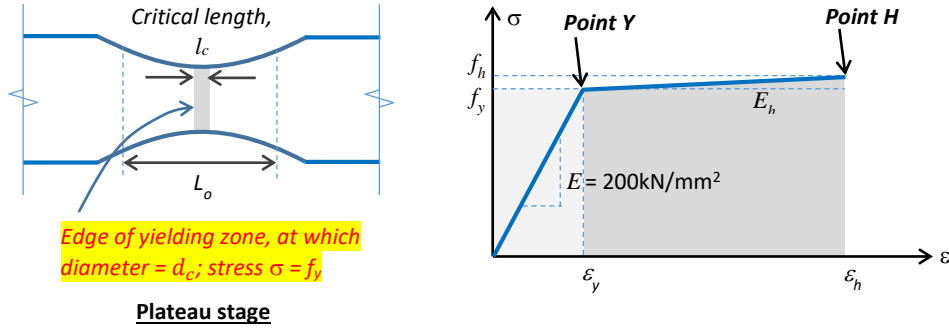


Figure 6. Yielding of funnel-shaped coupon at Plateau Stage

Stage 2 - Point of onset of hardening, H:

It should be noted that the total elongation of the coupon within the gauge length is composed of the elongation of the elastic zone and that of the yielding zone. For the elongation of the elastic zone, Equation (3) can be directly applied with an integral from l_c to d . For the elongation of the yielding zone, both deformations contributed by the elastic and the plateau stages should be taken into account. The simplified mathematical formulation is given by:

$$\Delta = \Delta_{elastic} + \Delta_{yielding}$$

$$\text{where } \Delta_{elastic} = \int_{l_c}^d \frac{f_h}{E} * \frac{\pi d^2}{4} * \frac{1}{\pi r^2} dl$$

$$\Delta_{yielding} = \int_0^{l_c} \frac{(f_h - f_y)}{E_h} * \frac{\pi d^2}{4} * \frac{1}{\pi r^2} dl + \int_0^{l_c} \frac{f_y}{E} * \frac{\pi d^2}{4} * \frac{1}{\pi r^2} dl$$

$$\text{where } E_h = 0.90 \text{ kN/mm}^2 \text{ as measured from test data}$$

After calculations as presented in Appendix A, the total deformation Δ is found to be 0.096mm. Hence, the engineering strain at the end of the plateau stage $\epsilon_h = \Delta / 10 \times 100\% = 0.96\%$, while the stress of Point H, $f_h = 767 \text{ N/mm}^2$.

2.3.2 Deformation at the hardening stage

After the onset of the hardening stage, deformations are highly localized in the minimum cross-section of the funnel-shaped coupon, and thus, the coupon undergoes a large amount of hardening leading to a very different longitudinal profile. Therefore, Equation (1) describing the longitudinal profile of the test coupon is no longer valid. Hence, the elongation of the coupon within the gauge length cannot be assessed using Equation (2).

Instead of using analytical solutions, digital image correlation method (Ho et al. 2018 and 2019) is applied to determine the point of the tensile strength. Figure 7 illustrates the measured instantaneous diameter of the funnel-shaped coupon under different deformations.

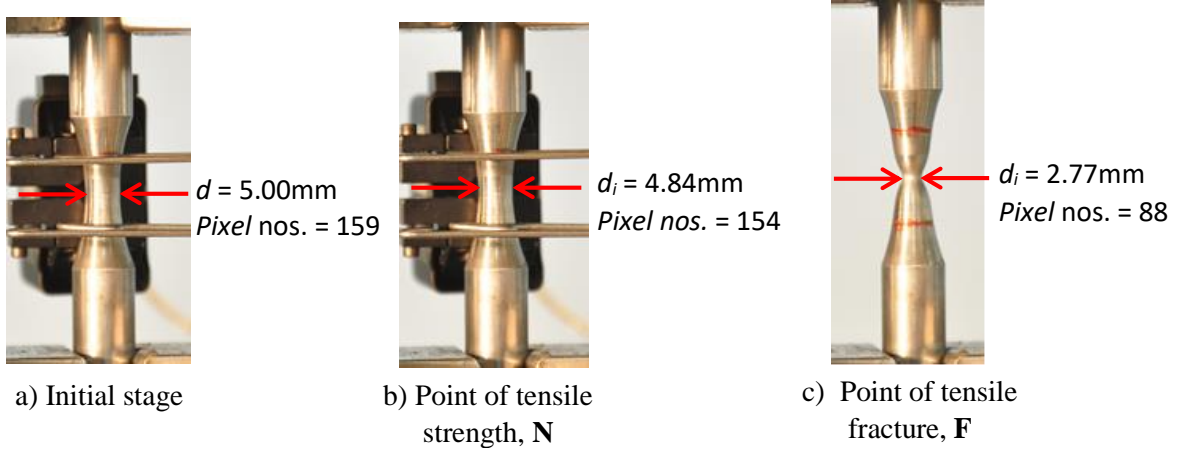


Figure 7. Measurement of instantaneous diameter of funnel-shaped coupon at different deformations

Stage 3 - Point of tensile strength (i.e. onset of necking), N:

At the point of tensile strength, the diameter of the coupon is reduced from 5.00mm to 4.84mm. Thus, the reduction ratio to the cross-sectional area is $4.84^2/5.00^2 = 0.939$. Accordingly,

True strain $\varepsilon = \ln(1/0.939) = 0.065 = 6.5\%$

Corresponding engineering strain $\varepsilon_u = e^\varepsilon - 1 = 6.7\%$

Tensile strength, $f_u = 798.6 \text{ N/mm}^2$ as measured from test data.

Stage 4 - Point of fracture, F:

After the onset of necking, the applied load decrease with the instantaneous area. Meanwhile, the deformation is highly localized in the necking region. From Point H to Point F, the total deformation is $\Delta_{neck} = 2d \cdot \varepsilon_L - 2d \cdot \varepsilon_h = 2.58 - 0.12 = 2.46\text{mm}$, and hence, $\varepsilon_{neck} = \Delta_{neck}/5d = 2.46/25 = 0.0984$. The total elongation $\varepsilon_L = \varepsilon_u + \varepsilon_{neck} = 0.0670 + 0.0984 = 0.1654 = 16.54\%$.

3. EFFECT OF NON-UNIFORM STRESSES AT THE FUNNEL-SHAPED REGION

According to the research studies by Bridgman (Bridgman 1952), the effect of non-uniform of stresses across the minimum cross sections of the funnel-shaped coupons should be taken into account. The non-uniformity of the stresses depends heavily on the ratio of $d/2R$ according to the following definitions:

d is the diameter of the minimum cross section of the funnel-shaped coupon as illustrated in Figure 2.

R is the radius of curvature of the longitudinal profile of the funnel-shaped coupon as illustrated in Figure 1b.

The stress correction factor, η_σ , is given by:

$$\eta_\sigma = 1/\left\{\left(1 + 4\frac{R}{d}\right)^{1/2} \ln\left[1 + \frac{d}{2R} + \left(\frac{d}{R}\right)^{1/2} \left(1 + \frac{d}{4R}\right)^{1/2}\right] - 1\right\} \quad (4)$$

In the current study, the ratio $d/2R = 0.083$ at small deformation range. Hence, the stress correction factor, η_σ , is equal to 0.95.

4. EQUIVALENT ENGINEERING STRESS-STRAIN CHARACTERISTICS

Based on the theoretical findings as presented in Sections 2 and 3, the equivalent engineering stress-strain characteristics to a cylindrical coupon is determined with details presented in Table 2.

Table 2. Equivalent engineering stress-strain characteristics of a funnel-shaped coupon

	Corrections	Corrected values (FUN01)	Measured values (CYD01)
Yield point (Y)	$f_y = 751 \times \eta_\sigma = 751 \times 0.95 =$	713.5 N/mm ²	711.0 N/mm ²
	$\varepsilon_y = f_y/E = 713.5/200000 =$	0.36%	0.36%
Hardening point (H)	$f_h = 767 \times \eta_\sigma = 767 \times 0.95 =$	728.7 N/mm ²	716 N/mm ²
	$\varepsilon_h = \varepsilon_y + \frac{(f_h - f_y)}{E_h}$ $= 0.0036 + \frac{(728.7 - 713.5)}{900} =$	2.04%	2.34%
Point of Tensile Strength (N)	$f_y = 789.6 \times \eta_\sigma = 789.6 \times 0.95 =$	750.1 N/mm ²	753.1 N/mm ²
	$\varepsilon_u = e^\varepsilon - 1 = e^{0.065} - 1$	6.70%	6.57%
Point of fracture (F)	$\varepsilon_L = \varepsilon_u + \varepsilon_{neck}$	16.5%	16.0%

5 VERIFICATION OF TRANSFORMATION RULES

In order to verify the proposed transformation rules, advanced numerical models of both funnel-shaped and cylindrical coupons are established using a measured true stress strain curve of cylindrical coupon CYD01 obtained by Instantaneous Area Method (Ho et al. 2009). Figure 8 plots both measured and predicted engineering stress strain curves in the same graph for direct comparison. It is shown that good agreements are achieved in terms of stress-strain characteristics and ductility for both funnel-shaped and cylindrical coupons.

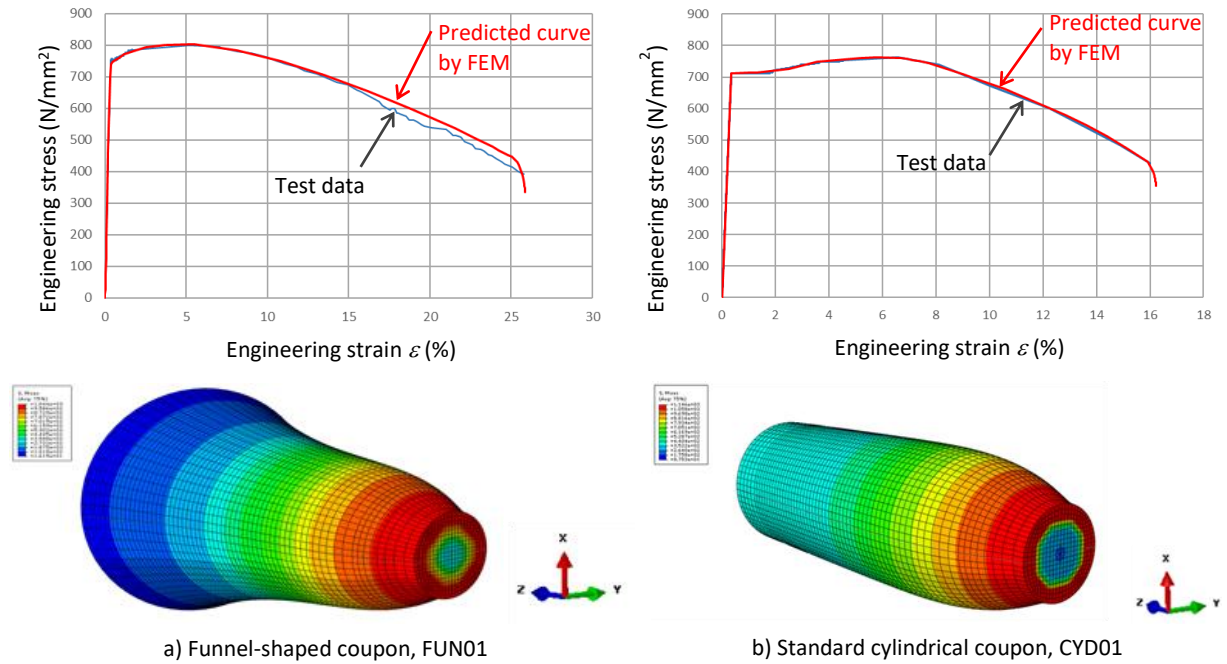


Figure 8. Numerical modeling on S690 steel funnel-shaped and cylindrical coupons

6 CONCLUSIONS

This paper presents a theoretical study into the correlation on the stress strain characteristics between a funnel-shaped coupon and a standard cylindrical coupon. A series of transformation formulae are proposed for various deformation ranges, namely i) Elastic range; ii) Plateau range; iii) Hardening range; and iv) Necking range. The test results provide strong evidence to the effectiveness of the proposed transformation rules. The research findings are considered to be very important to subsequent investigations into the hysteretic behaviour of the S690 steels.

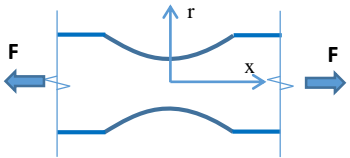
ACKNOWLEDGEMENTS

The project leading to publication of this paper is partially funded by the Research Grants Council of the Government of Hong Kong SAR (Project No. PolyU 5148/13E, PolyU 152194/15E, and PolyU 152687/16E) and the Research Committee of the Hong Kong Polytechnic University (Project No. RTZX). Both technical and financial support from the Chinese National Engineering Research Centre for Steel Construction (Hong Kong Branch) (Project No. 1-BBY3 & 6) of the Hong Kong Polytechnic University is also gratefully acknowledged. Special thanks go to the Nanjing Iron and Steel Company Ltd. in Nanjing for supply of high strength steel materials.

REFERENCES

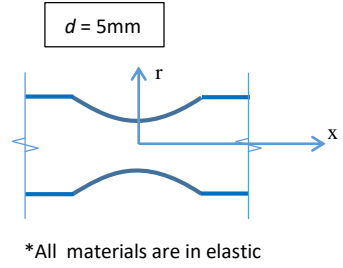
- Bridgman P. (1952), *Studies in Large Plastic and Fracture*, McGraw-Hill, New York, NY, USA.
- BS 3518-3 (1963), *Method of fatigue testing – Part 3: Direct stress fatigue tests*. British Standards Institution.
- BS EN ISO 6892-1 (2009), *Metallic materials – Tensile testing Part 1: Method of test at ambient temperature*. British Standards Institution.
- Fournier, B., Sauzay M., Caes, C., Noblecourt M., and Mottot, M. (2006), Analysis of the hysteresis loops of a martensitic steel – Part I: Study of the influence of strain amplitude and temperature under pure fatigue loadings using an enhanced stress partitioning method, *Materials Science and Engineering A*, 437, 183-196.
- FEMA-461 (2007), *Interim testing Protocols for determining the seismic performance characteristics of structural and non-structural components*. Federal Emergency Management Agency.
- GB/T 15248 (1994), *Metallic Materials – Constant Amplitude Strain Controlled Axial Fatigue – Method of Test*. Standard Press of China, Beijing, China. (In Chinese)
- Ho H.C., Chung K.F., Liu X., Xiao M. and Nethercot D.A. (2019). Modelling tensile tests on high strength S690 steel materials undergoing large deformations. *Engineering Structures*, 192:305-322.
- ISO 12106 (2003), *Metallic materials – Fatigue testing – Axial-strain-controlled method*. International Organization for Standardization.
- Khan S., Wilde F., Beckmann F., and Mosler J. (2012), Low cycle fatigue mechanism of the lightweight alloy Al2024, *International Journal of Fatigue*, 38, 92-99.
- Nip, K. H., Gardner, L., Davies, C. M., and Elghazouli, A. Y. (2010), Extremely low cycle fatigue tests on structural carbon steel and stainless steel, *Journal of Constructional Steel Research*, 66, 96-110.

APPENDIX A – CALCULATION PROCEDURES FOR DEFORMATIONS OF FUNNEL-SHAPED COUPONS AT DIFFERENT DEFORMATION STAGES

General formula of deformation of funnel-shaped coupon	
$\Delta = \sum \frac{\sigma}{E} = \int \frac{F}{EA} dx$ $= \int \frac{F}{E\pi r^2} dx \quad \text{where } r = \frac{d}{2} + R - \sqrt{R^2 - x^2}$ $= \int \frac{F}{\pi E} \frac{1}{\left(\frac{13d}{2} - \sqrt{36d^2 - x^2}\right)^2} dx$	

1. Deformation at the point of yielding, **Y**

$$\begin{aligned}\Delta &= 2 \int_0^d \frac{F}{\pi E} \frac{1}{\left(\frac{13d}{2} - \sqrt{36d^2 - x^2}\right)^2} dx \\ &= \int_0^5 \frac{F}{\pi E} \frac{2}{\left(\frac{13d}{2} - \sqrt{36d^2 - x^2}\right)^2} dx \\ &= 0.459 \frac{f_y \pi d^2}{E} = 0.459 \frac{14760}{200000} = 0.034 \text{ mm}\end{aligned}$$

2. Deformation at the point of onset of hardening, **H**

Determine the critical diameter d_c by using the principle of force equilibrium:

$$\begin{aligned}\frac{\pi d_c^2}{4} \cdot f_y &= \frac{\pi d^2}{4} \cdot f_h \\ \therefore \text{critical diameter } d_c &= d \sqrt{f_h/f_y}\end{aligned}$$

By putting the value of critical radius, $d_c/2$, into Equation (1), the critical length of yielding zone, l_c , is given by:

$$\therefore \text{critical length } l_c = 0.35L_o$$

Determine the total deformation

$$\Delta = \Delta_{\text{elastic}} + \Delta_{\text{yielding}}$$

$$\text{where } \Delta_{\text{elastic}} = \int_{l_c}^d \frac{f_h}{E} * \frac{\pi d^2}{4} * \frac{1}{\pi r^2} dx$$

$$= \int_{l_c}^d \frac{f_h d^2}{4E} * \frac{1}{\left(\frac{13d}{2} - \sqrt{36d^2 - x^2}\right)^2} dx$$

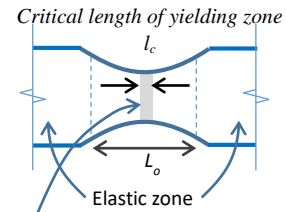
$$\begin{aligned}\Delta_{\text{yielding}} &= \int_0^{l_c} \frac{(f_h - f_y)}{E_h} * \frac{\pi d^2}{4} * \frac{1}{\pi r^2} dx \\ &\quad + \int_0^{l_c} \frac{f_y}{E} * \frac{\pi d^2}{4} * \frac{1}{\pi r^2} dx\end{aligned}$$

$$= \int_0^{l_c} \frac{(f_h - f_y) d^2}{4E_h} * \frac{1}{\left(\frac{13d}{2} - \sqrt{36d^2 - x^2}\right)^2} dx$$

$$+ \int_0^{l_c} \frac{f_y d^2}{4E} * \frac{1}{\left(\frac{13d}{2} - \sqrt{36d^2 - x^2}\right)^2} dx$$

$$\begin{aligned}\Delta &= 5.57 \frac{f_h}{E} + 3.45 \left[\frac{(f_h - f_y)}{E_h} + \frac{f_y}{E} \right] \\ &= 5.57 \cdot \frac{767}{200000} + 3.45 \cdot \left[\frac{16}{900} + \frac{751}{200000} \right] \\ &= 0.0214 + 0.0743 \\ &= 0.0957 \text{ m}\end{aligned}$$

At the minimum cross section:
diameter = d ; stress $\sigma = f_h$



Edge of yielding zone, at which
diameter = d_c ; stress $\sigma = f_y$

